Journal of Petroleum Science and Engineering 208 (2022) 109670

Contents lists available at ScienceDirect

Journal of Petroleum Science and Engineering

journal homepage: www.elsevier.com/locate/petrol

Source rock with high abundance of C_{28} regular sterane in typical brackish-saline lacustrine sediments: Biogenic source, depositional environment and hydrocarbon generation potential in Junggar Basin, China

Shiju Liu [a,b], Gang Gao [a,b,*], Jun Jin [c], Wenzhe Gang [a,b], Baoli Xiang [c]

[a] College of Geosciences, China University of Petroleum, No.18 Fuxue Road, Beijing, 102249, China
[b] State Key Laboratory of Petroleum Resource and Prospecting, China University of Petroleum, No.18 Fuxue Road, Beijing, 102249, China
[c] Experimental Testing Institute, Xinjiang Oil Field Company, Karamay, Xinjian, 834000, China

ARTICLE INFO

Keywords:
Biogenic origin
Biomarkers
Sterane
Sedimentary environment
Hydrocarbon generation

ABSTRACT

In the brackish water sedimentary environment of the Junggar Basin in Xinjiang, the organic-rich shale and shale oil formation with relatively low maturity, is characterized by relatively high abundance of C_{28} regular steranes. However, the biogenic source of organic matter and favorable sedimentary environment for the type of source rock has been thoroughly classified. In this paper, organic geochemical and petrological, analyses of the Lucaogou Formation shale in the Jimusaer Sag, Junggar Basin in the north of Xinjiang Uygur Autonomy Region were carried out. The source rocks in the Lucaogou Formation are mainly composed of two types of maceral including lamalginite (cyanobacteria) and telalginite (green algae), with the former predominantly fueling the high C_{28} regular sterane content. Petrological, organic and inorganic geochemical analyses suggest that the lamalginite was developed in low-salinity water while the telalginite was developed in high-salinity water. Based on geochemical and organic petrological characteristics, both the lamalginite and telalginite have good hydrocarbon-generating potential, but in the lower thermal evolution stage of the Lucaogou Formation source rock, telalginite have higher hydrocarbon-generating rate.

1. Introduction

The C_{27}, C_{28}, and C_{29} regular steranes can be used to distinguish biogenic sources of organic matter (Volkman, 1986; Patterson, 1994; Nes and Venkatramesh, 1994; Volkman et al. 1994, 1998, 2003, 2005). According to previous studies, C_{27} steranes are related to aquatic planktonic algae (Huang and Meinschein, 1979), C_{28} regular steranes are related to diatoms of thorny-source type (Grantham and Wakefield, 1988), C_{29} steranes are related to higher plants and in some cases, from green and brown macro- and microalgae (Moldowan, 1985). Previous data showed that the relative content of C_{28} regular steranes in marine crude oil increases during the geological records (Grantham and Wakefield, 1988). This correlate with the relative increase in the contribution of diatoms, coccolithophores and dinoflagellates and the diversity of algae (Fig. 1). The abovementioned phenomena occur in marine crude oil, but the sources of some compounds are still controversial. It is difficult to find the laws demonstrated by the phenomena, because there are variances in the environments and areas (Volkman, 1986; Patterson, 1994; Nes and Venkatramesh, 1994; Volkman et al., 1998). The high content of sterane series with C_{28}-carbon skeleton have been found in shales from different saline lacustrine basins, such as Green River shale, shales of Fengcheng and Lucaogou Formations in Xinjiang, Northwest China and Es1 member in Qikou Sag in the Bohai Bay Basin (Horsfield et al., 1994; Meng et al., 2011; Gao et al., 2016; Cao et al., 2020). Zhang et al. (2020) suggest that the high C_{28} steranes were produced by algae blooming in the water column of a mixing lacustrine environment based on isotope studies. However, study of the biogenic source of C_{28} regular sterane in the Lucaogou Formation is limited.

The Permian source rocks are the primary source rocks in the Junggar Basin (Fig. 2) (Kuang et al., 2012) and the source rocks of the Lucaogou Formation in the Jimusaer Sag are considered as world-class and of high-quality (Carroll, 1998; Xie et al., 2015; Liu et al., 2017). In this paper, the source rocks of the Lucaogou Formation in the Jimusaer Sag were systematically sampled. Petrology, molecular geochemistry and scanning electron microscope (SEM) were used to determine the sources of C_{28} regular steranes in the source rocks and their

* Corresponding author. College of Geosciences, China University of Petroleum, No.18 Fuxue Road, Beijing, 102249, China.
E-mail address: gaogang2819@sina.com (G. Gao).

https://doi.org/10.1016/j.petrol.2021.109670
Received 30 April 2021; Received in revised form 14 September 2021; Accepted 11 October 2021
Available online 20 October 2021

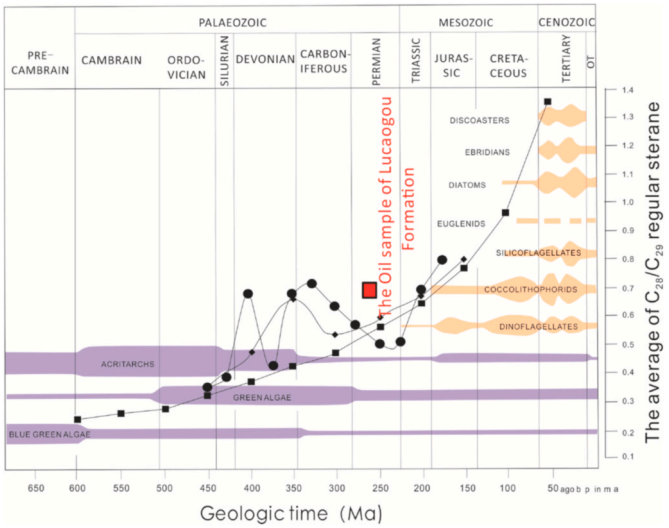

Fig. 1. C_{28}/C_{29}-sterane ratio of the oil sample of the Lucaogou Formation (Red filled squares, Table 2) compared with 500 rock samples, averaged in 50 Ma steps (rhomboids), in 25 Ma steps (filled circles) by Lorenz and Petra (2006) and 400 oil sample (squares) analyzed by Grantham and Wakefield (1988). (For interpretation of the references to color in this figure legend, the reader is referred to the Web version of this article.)

hydrocarbon generation potential.

2. Geological setting

The Junggar Basin located in the Kazakhstan Plate and an important part of the central Asian orogenic belt, is a large oil and gas basin in western China (Yi et al., 2018). The Jimusaer Sag is located in the southwest margin of the eastern uplift of the basin, with an area of about 1300 km^2. It is bounded by faults in all directions except the east, the strata in the sag gradually thins towards the east and pinched out in the Guxi Uplift (Fig. 2A and B). The structural framework of the sag is severely affected by the surrounding boundary fault and structural style of the Carboniferous basement, resulting in the formation of a dustpan-shaped sag with fault in the west and overlapped strata in the east (Fang et al., 2005; Yi et al., 2018).

The Guadalupian Lucaogou Formation is a set of fine-grained hybrid sedimentary rock (Zhang et al., 2018), which is characterized by the coexistence of diverse components including terrigenous clastic, volcanic material and lacustrine carbonate. The rock types are complex, including mudstone, siltstone, dolomite, and pyroclastic rocks (Gao et al., 2016). The Lucaogou Formation source rock is rich in oil-prone organic matter and entered the oil generation window, showing wide distribution throughout the sag (Gao et al., 2016; Bai et al., 2016).

3. Sample and methods

3.1. Sample

Exactly 27 shale samples belonging to the Lucaogou Formation (P_2l) were obtained between depths 3500–3640m in Well A situated in the Jimusaer Sag of the Junggar Basin (Fig. 2C). Samples were selected based on sedimentary structure, palaeontological and hand-detected density characteristics of the core samples. All of the samples were subjected to the following analyses.

3.2. Method

3.2.1. Total organic carbon (TOC) and Rock-Eval pyrolysis

The TOC of the rock samples was determined using a Leco CS-230 analyzer. Rock-Eval pyrolysis was conducted with an OGE-II rock pyrolyzer which was developed by the Research Institute of China Petroleum Exploration and Development. The test standard follows the State Standard of the People's Republic of China (Gao et al., 2016). Parameters measured by the Rock-Eval pyrolysis tool include S_1, S_2, and Tmax (Espitalié et al., 1985; Peters, 1986; Peters and Cassa, 1994). S_1 represents some free hydrocarbons that can be volatilized (mg HC/g rock) at 300 °C. S_2 represents the amount of hydrocarbons (mg HC/g rock) that are expelled from the rock during temperature-programmed pyrolysis (300–600 °C). Tmax is the temperature when the maximum rate of pyrolysis occurs. Source rock parameters such as Production Index (PI = $S_1/[S_1 + S_2]$) and Hydrogen Index (HI = $[S_2/TOC] \times 100$; mg HC/g TOC) were calculated from these measured parameters.

3.2.2. Petrographic analyses

The core samples were prepared for mineralogical analyses and macerals identification under the microscope. The samples were cut perpendicular to bedding into blocks and were polished on a Buehler automatic grinding and polishing machine (EcoMet 250 with AutoMet 250) to give a smooth surface. The macerals were observed with the Leica microscope (DM6 M LIBS) under reflected and fluorescent lights. The quantification method described in Liu et al. (2017) was used to quantify microscopic components.

3.2.3. SEM analyses

Representative samples for SEM analysis were selected based on observation from thin sections and organic petrographic analyses. The samples were coated with gold and analyzed on a Hitachi SU8010 field emission SEM-EDS. Specimens with a natural fracture surface facing upwards were examined in a FEI-Philips ESEM-FEG Quanta 200 F scanning electron microscope at 20 kV. These analyses were conducted at the State Key Laboratory of Petroleum Resource and Prospecting at the China University of Petroleum (Beijing).

3.2.4. Gas chromatography and gas chromatography–mass spectrometry

The Gas chromatography and gas chromatography–mass spectrometry analyses were conducted as described by Gao et al. (2016). All samples were extracted with $CHCl_3$ for 72 h in a Soxhlet apparatus. The extract was subjected to open silica gel column chromatography with n-hexane to obtain saturated hydrocarbon, aromatic hydrocarbon, non-hydrocarbon and asphaltene components. Gas chromatography (GC) and gas chromatography-mass spectrometry (GC-MS) were used to analyze the molecular geochemical composition of saturated hydrocarbons. Gas chromatography (GC) analysis was carried out using the HP6890 gas chromatograph apparatus, which is equipped with HP-5 chromatographic column with inner diameter 30 m × 0.32 mm, film thickness 0.25 μm. Nitrogen was used as carrier gas and the column temperature was initially held at 80 °C for 5 min, then increased from 80 °C to 290 °C at 4 °C/min, and then held it constant for 30 min. The Agilent 7890-5975c gas chromatography-mass spectrometry was used for GC-MC analysis, with helium as the carrier gas at a rate or 1 mL/min. The GC temperature was initially held at 50 °C for 1 min, then increased at to 100 °Cat the rate of 20 °C/min, and then kept it constant for 3 min, then increased to 300 °C at a rate of 2.6 °C/min, and then kept at 300 °C for 30 min.

3.2.5. Inorganic geochemical analyses

Samples were dried in the airing chamber, and ground into a 200-mesh with an agate mortar. The powdered samples were placed in an oven and dry for 12 h at 105 °C. 10 mg of the powdered sample was placed on the Teflon copple by adding 1–2 drops of high-purity water to moisturize the powdered sample. Then 1 ml high-purity Nitric acid and 1 ml high-purity hydrofluoric acid was added. The Teflon copple was placed in a steel sleeve, tightened and placed in an oven at 190 °C for more than 48 h. The dissolved sample was allowed to cool, the lid was opened and placed on an electric hot plate to evaporate at 140 °C. then

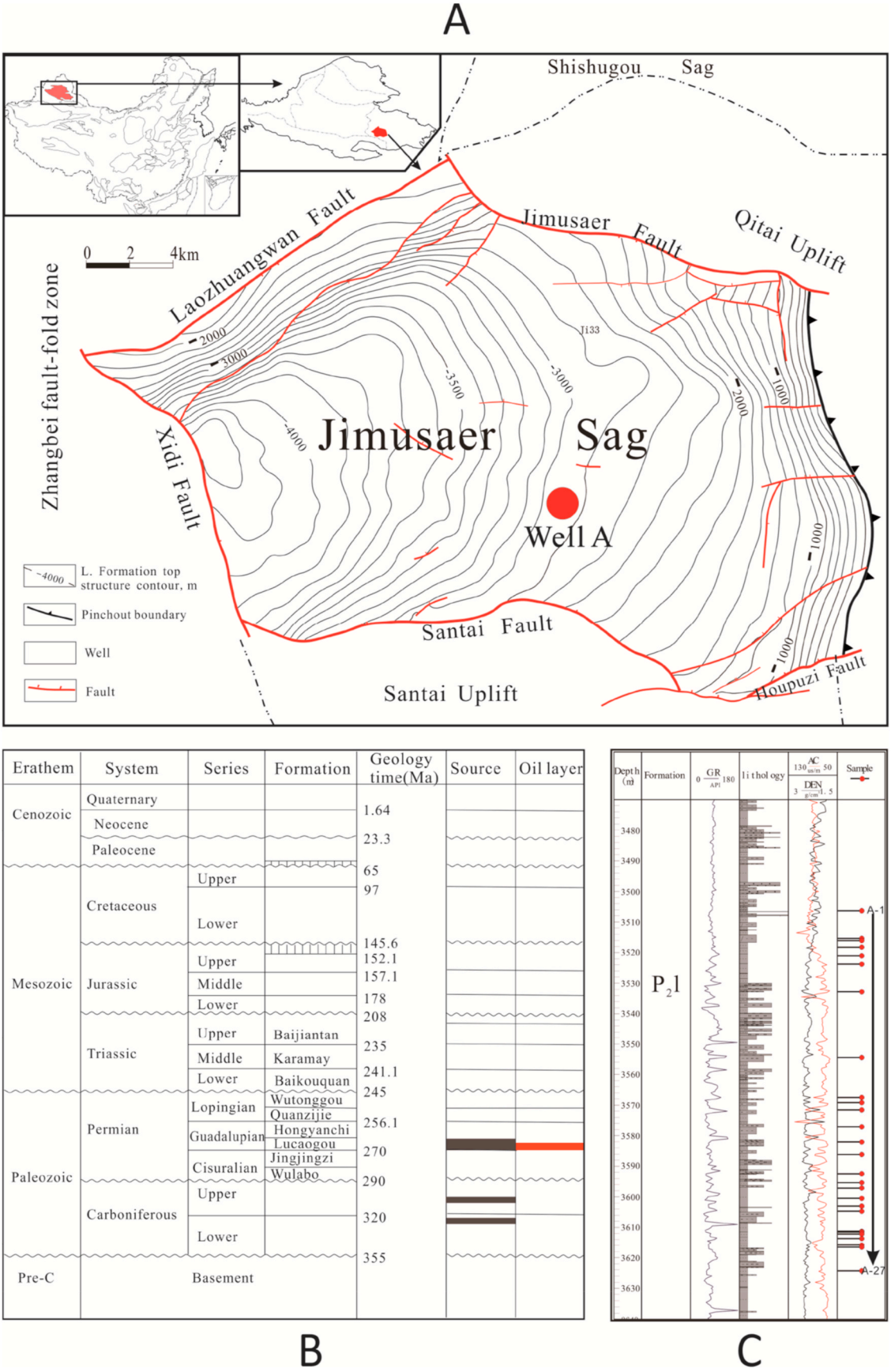

Fig. 2. Locality (A), Stratigraphic column (B) and sample point in Well A (C) of the Jimusar sag in Junggar Basin. (modified from Gao et al., 2016).

add 1 ml of Nitric acid and evaporate to dryness again to ensure that the Teflon copple wall is free of liquid. Add 3 ml nitric acid with a concentration of 30%, put Teflon into the steel sleeve again, tighten it and put it in a ten oven at ten 190 °C for 12 h. Transfer the solution into a polyethylene bottle and dilute it with 2% nitric acid. The prepared samples were analyzed using the inductively coupled plasma mass spectrometer (ICP-MS) NexION300D. Testing was completed at the State Key Laboratory of Geological Process and Mineral Resources of Beijing Institute of Nuclear Industry.

4. Result

4.1. TOC and Rock–Eval pyrolysis

The TOC content and Rock-Eval pyrolysis results for the Lucaogou Formation samples penetrated by Well A are presented in Table 1. The TOC values of the studied shales varies between 1.25% and 30.1% (Table 1, Fig. 3A). The Rock-Eval pyrolysis parameters S_1, S_2 and PG=S_1+S_2 are between 0.09 and 4.04, 5.88 and 195.82 and 5.97 and 197.23 with means of 1.28, 51.93 and 53.21 (mg HC/g rock), respectively (Table 1, Fig. 3C and D). The PI (S_1/(S_1+S_2)) values range from 0.01 to 0.09, with a mean of 0.03 (Table 1). Rock-Eval Tmax values range from 436 to 457 °C (averaging 446 °C; Table 1). HI values were in the range of 358–823 mg HC/g TOC (mean: 659 mg HC/g TOC) (Table 1, Fig. 3B).

4.2. Petrographic and organic petrographic analyses

Petrological characteristics record the heterogeneity of deposition and diagenesis and retain the original sedimentary environment that can be used for rough evaluation (Frimmel, 2008; Zhang et al., 2014). From the observation of core samples and thin sections, the Lucaogou Formation in the Jimusaer is mainly composed of quartz, feldspar, and carbonates (Fig. 4C, F and I), coupled with the occurrence of fossils, pyrite, gray limy lamina seen as strips on handpicked samples (Table 1, Fig. 6A and B).

From organic petrologic analyses, the morphology, quantity, size, and fluorescence of bio-precursors were characterized in the tested samples (Luo et al., 2018). Polished and thin sections examination under the petrological microscopic show alginite, which can be further classified into lamalginite (Fig. 4G, Fig. 5A), telalginite (Fig. 4A and D) and MBG (mineral bituminous groundmass) (Fig. 5G and H). There were vitrinite and inertinite derived from higher plants in each sample (Fig. 4B, E and H), which were in low contents generally and indicated the dominant organic matter source from phytoplankton, being consistent with higher HI values demonstrated in the diagram in Table 1. Lamalginite are composed of thin-walled clusters or single-celled algae that usually appear as distinct laminae, but usually have no recognizable biogenic structure under transmitted light (Hutton, 1987) (Fig. 4G, Fig. 5A, B and E). The studied samples contained largely varying concentrations of lamalginite, which has a particular biogenic structure and orange-brown fluorescence (Table 1) (Fig. 4A and D, Fig. 5G and H). The telalginite is thought to be derived from green algae (plankton) reported in the Lucaogou Formation of the Santanghu Basin (Hackley et al., 2016). MBG (mineral-bituminous groundmass) is the amorphous fine-grained organic-inorganic matter mixture, which is an important structure for organic matter enrichment in the study. The MBG is possibly sourced from the primary fine dispersive organic matter and contemporaneous organic matter from mechanical breakdown and biodegradation in the sedimentary-early diagenesis stage. In the studied samples, the MBG can be ubiquitously observed in most samples (Table 1).

4.3. Aliphatic hydrocarbons

The *n*-alkane distribution is unimodal with a maximum at *n*-C_{21}, *n*-

Table 1
Meassured data of TOC, Rock-Eval parameters and maceral contents (vol%) for shale samples in the studied area.

Sampes	Depth (m)	Core features	TOC (%)	Tmax (°C)	S_1(mg HC/g rock)	S_2(mg HC/g rock)	HI (mg HC/g TOC)	PI	PG	Lipt.(vol%, mmf)			Vitr.(vol %, mmf)	Inert. (vol%, mmf)
										telalginite	lamalginite	MBG		
A-1	3506.31		1.86	448	0.38	6.65	358	0.05	7.03	62	4	10	7	17
A-2	3515.35		7.76	444	2.95	48.99	631	0.06	51.94	67	4	11	8	10
A-3	3516.05		5.31	441	2.89	28.77	542	0.09	31.66	83	2	2	7	6
A-4	3518.25		6.19	445	1.99	40.36	652	0.05	42.35	80	2	3	6	10
A-5	3521.03	Oil-rich	8.75	440	4.04	42.81	489	0.09	46.85	72	2	6	10	10
A-6	3523.78		6.66	444	1.21	42.7	641	0.03	43.91	69	5	8	10	8
A-7	3532.79		6.37	446	0.71	52.38	822	0.01	53.09	44	43	0	6	7
A-8	3554.51		4.07	445	0.65	26.91	661	0.02	27.56	31	55	0	4	10
A-9	3567.5	Con.	30.1	457	1.49	188.1	625	0.01	189.59	0	77	0	10	13
A-10	3569.2		5.22	449	0.41	40.19	770	0.01	40.6	12	73	0	3	12
A-11	3571.6		2.33	442	0.66	9.19	394	0.07	9.85	2	79	0	12	8
A-12	3577.1	Con.	25.1	452	1.41	195.82	780	0.01	197.23	0	94	0	1	6
A-13	3582.1		12.9	450	1.21	100.49	779	0.01	101.7	17	59	0	10	14
A-14	3586.2	Con.	7.8	448	0.78	64.17	823	0.01	64.95	0	93	0	0	6
A-15	3592.45		1.25	447	0.09	5.88	470	0.02	5.97	20	70	0	5	5
A-16	3595.4	Con. & Fish	6.06	447	2.01	40.66	671	0.05	42.67	3	71	0	10	15
A-17	3597.1		4.12	449	0.72	27.43	666	0.03	28.15	46	10	19	10	15
A-18	3600.5	a little con.	6.01	448	0.77	39.79	662	0.02	40.56	48	11	22	9	11
A-19	3603.05	Pyrite	7.04	451	0.8	55.31	786	0.01	56.11	50	7	29	4	10
A-20	3604.75	Con.	3.29	436	1.2	24.44	743	0.05	25.64	4	73	10	2	10
A-21	3611.25		4.22	450	0.85	33.27	788	0.02	34.12	67	17	9	2	5
A-22	3611.55		6.58	448	0.97	51.86	788	0.02	52.83	45	10	20	7	18
A-23	3612.15		3.52	442	0.62	18.81	534	0.03	19.43	39	0	34	10	17
A-24	3613.7		11.6	444	1.9	87.49	754	0.02	89.39	3	77	6	5	9
A-25	3615.8	Pyrite	5.99	442	0.7	38.87	649	0.02	39.57	41	4	30	9	17
A-26	3616.55	Pyrite	1.47	447	0.26	8.55	582	0.03	8.81	68	0	15	8	9
A-27	3624.3		11.3	444	2.98	82.09	727	0.04	85.07	37	28	18	6	10

Note: Core features: Observation characteristics of hand specimens; Con.: Conchostracans; Fish: Fish remain; PI: S_1/(S_1+S_2); PG: S_1+S_2; Lipt.: Liptinite; Vitr.: Vitrinite; Inert.: Inertinite; vol%: volume percent; mmf: mineral-matter-free.

Table 2
Aliphatic hydrocarbon and trace element parameters of the Lucaogou Fm in this study.

Sampes	Depth(m)	Fm.	Lithology	1	2	3	4	5	6	7	8	9	10	11	12	13	14	15
A-1	3506.31	P_2l	mudstone	1.12	0.58	0.41	0.05	0.054	0.28	0.06	0.67	0.56	29.86	25.28	44.86			
A-2	3515.35	P_2l	mudstone	0.80	0.98	1.13	0.13	0.257	1.17	0.13	0.63	0.64	25.69	29.12	45.19	295	0.79	3.73
A-3	3516.05	P_2l	mudstone	0.80	1.15	1.33	0.15	0.344	1.09	0.10	0.57	0.64	28.30	28.04	43.66	316	0.81	3.33
A-4	3518.25	P_2l	mudstone	1.30	1.62	1.28	0.20	1.838	2.05	0.12	0.67	0.46	31.74	21.39	46.87	270	0.77	3.03
A-5	3521.03	P_2l	mudstone	1.37	1.80	1.35	0.19	0.972	1.63	0.18	0.70	0.51	31.05	23.29	45.67			
A-6	3523.78	P_2l	mudstone	1.14	1.50	1.11	0.16	0.209	1.44	0.11	0.84	0.60	34.91	24.46	40.63	90.8	0.69	2.88
A-7	3532.79	P_2l	mudstone	0.95	0.64	0.64	0.09	0.100	0.50	0.10	0.38	0.67	16.07	33.56	50.37			
A-8	3554.51	P_2l	mudstone	0.97	0.46	0.42	0.08	0.033	0.47	0.08	0.40	0.89	14.75	40.25	45.00			
A-9	3567.5	P_2l	mudstone	1.10	0.30	0.21	0.02	0.0001	0.33	0.09	0.37	1.19	13.86	46.88	39.26	89.4	0.64	1.72
A-10	3569.2	P_2l	mudstone	1.22	0.67	0.55	0.06	0.0001	0.42	0.10	0.30	0.94	12.61	42.29	45.10			
A-11	3571.6	P_2l	mudstone	1.22	0.14	0.07	0.01	0.0001	0.46	0.08	0.41	1.11	15.62	44.42	39.96			
A-12	3577.1	P_2l	mudstone	1.38	0.19	0.13	0.01	0.0001	0.28	0.09	0.69	1.21	22.78	42.33	34.89	108	0.66	2.24
A-13	3582.1	P_2l	mudstone	0.88	0.39	0.30	0.03	0.0001	1.55	0.38	0.28	0.71	11.49	36.87	51.64			
A-14	3586.2	P_2l	mudstone	0.79	0.24	0.17	0.02	0.0001	0.60	0.06	0.36	1.38	11.47	51.28	37.26	119	0.75	2.04
A-15	3592.45	P_2l	mudstone	0.50	0.33	0.20	0.03	0.0001	0.54	0.06	0.46	0.90	17.52	38.98	43.50	154	0.70	2.54
A-16	3595.4	P_2l	mudstone	0.92	0.33	0.21	0.03	0.0001	0.86	0.14	0.37	0.99	13.93	42.91	43.16	130	0.73	2.20
A-17	3597.1	P_2l	mudstone	1.22	0.67	0.55	0.06	0.0001	1.09	0.10	0.83	0.73	32.56	28.36	39.08			
A-18	3600.5	P_2l	mudstone	0.90	0.54	0.37	0.05	0.069	1.18	0.19	0.52	0.74	21.52	33.25	45.23	139	0.71	2.68
A-19	3603.05	P_2l	mudstone	1.30	0.60	0.40	0.07	0.0001	1.38	0.29	0.44	0.78	16.95	36.30	46.75	144	0.61	2.21
A-20	3604.75	P_2l	mudstone	1.34	0.57	0.39	0.05	0.0001	0.71	0.18	0.55	1.00	21.03	39.55	39.42			
A-21	3611.25	P_2l	mudstone	1.30	0.76	0.55	0.06	0.0001	1.32	0.16	0.36	0.82	14.21	38.62	47.17	138	0.68	1.94
A-22	3611.55	P_2l	mudstone	0.74	0.83	0.59	0.07	0.0001	1.34	0.16	0.35	0.76	14.57	36.87	48.55			
A-23	3612.15	P_2l	mudstone	0.74	0.83	0.59	0.07	0.195	1.45	0.19	0.34	0.69	13.89	35.07	51.04			
A-24	3613.7	P_2l	mudstone	1.29	0.72	0.54	0.07	0.0001	0.89	0.10	0.48	0.90	18.90	38.37	42.73			
A-25	3615.8	P_2l	mudstone	1.02	0.74	0.56	0.07	0.110	1.09	0.16	0.45	0.70	18.33	33.67	48.00	141	0.72	2.76
A-26	3616.55	P_2l	mudstone	0.97	0.93	0.75	0.11	0.143	1.46	0.22	0.40	0.66	16.88	32.96	50.16	172	0.75	2.47
A-27	3624.3	P_2l	mudstone	1.12	0.83	0.67	0.10	0.063	1.40	0.15	0.43	0.80	17.13	36.96	45.91	155	0.71	2.46
AO-1	3552.00 ~ 3564.00	P_2l	Oil	1.20	0.84	0.77	0.11	0.34	–	0.18	0.29	0.67	15.89	33.99	50.25			

Note: 1: Pr/Ph; 2: Pr/n-C_{17}; 3: Ph/n-C_{18}; 4: i-C_{21}/n-C_{19}; 5: β-carotane/n-Cmax; 6: C_{30}Hopane/n-Cmax; 7: Gammacerane/C_{30}Hopane; 8: C_{27}/C_{29}(C_{27}/C_{29} regular sterane); 9: C_{28}/C_{29}(C_{28}/C_{29} regular sterane); 10: C_{27}%($C_{27}/(C_{27}+C_{28}+C_{29})$ regular sterane); 11: C_{28}%($C_{28}/(C_{27}+C_{28}+C_{29})$ regular sterane); 12: C_{29}%($C_{29}/(C_{27}+C_{28}+C_{29})$ regular sterane); 13: boron content (ppm); 14:V/Cr; 15:V/(V + Ni).

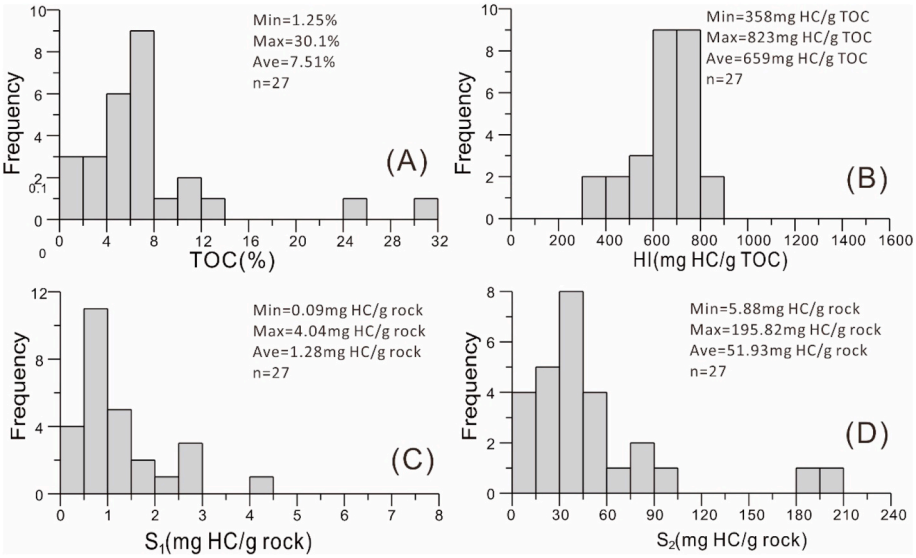

Fig. 3. Histograms of (A) TOC, (B) HI, (C) S_1 and (D) S_2 in the studied samples.

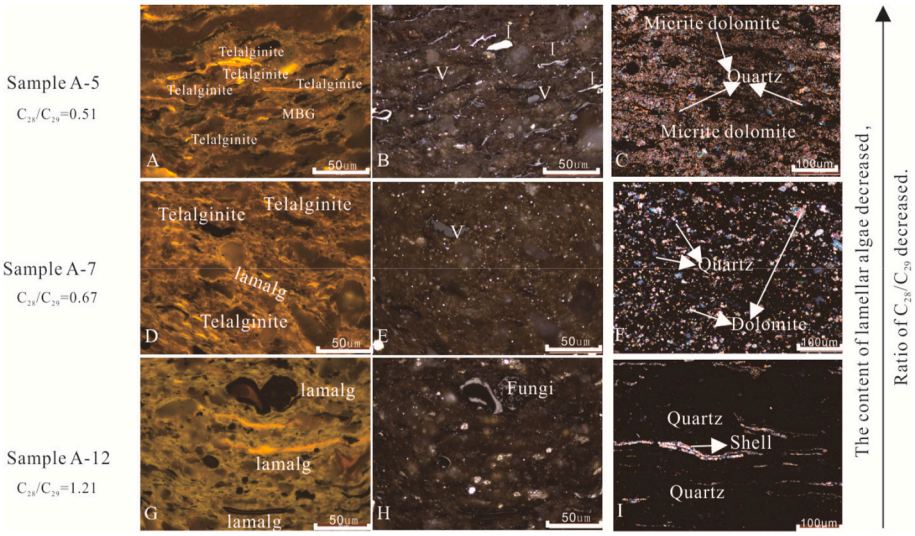

Fig. 4. Organic petrological characteristics of typical samples. The observed samples were all along the vertical bedding plane. A, B, D, E, G and H are taken under oil immersion. A: brightly fluorescent telalginite with orange color under fluorescent light (3521.03 m depth); B: same field as (A) under reflected light; C: Thin-section photograph showing A lot of micritic dolomite and a little quartz under cross-polarized light; D: brightly fluorescent telalginite and lamalg with orange color under fluorescent light (3532.79 m depth); E: the same field as (D) under reflected light; F: Thin-section photograph showing dolomite and quartz under cross-polarized light; G: brightly fluorescent lamalg with green yellow color under fluorescent light (3577.1 m depth); H: same field as (G) under reflected light; I: Thin-section photograph showing shell and quartz under cross-polarized light. (For interpretation of the references to color in this figure legend, the reader is referred to the Web version of this article.)

C_{23}, or *n*-C_{25} in all samples (Fig. 7). The studied shales contain variable ratios of Pr/*n*-C_{17} (0.14–1.80, mean: 0.72), Ph/*n*-C_{18} (0.07–1.35, mean: 0.57) and *i*-C_{21}/n-C_{19} (0.01–0.2, mean: 0.07). The Pr/Ph ratios ranged between 0.50 and 1.38 (mean: 1.05). *β*-carotane is generally derived from carotene, which can be easily oxidized and is generally difficult to be preserved in organic matter. It is generally identified in $M/Z = 125$ spectrum, and the content on TIC was basically low, or it is not displayed. The existence of *β*-carotane in the sample in the study can be clearly observed in TIC, indicating that it has a relatively high content of β-carotane. A high abundance of *β*-carotane was observed in some samples, as suggested by the ratio of *β*-carotane/n-C_{max} (*β*-carotane/*n*-alkane with the highest concentration) (Fig. 7 and Table 2). All samples contain abundant pentacyclic terpanes, and the high abundance of C_{30} αβ-hopane was observed in *TIC* diagram, as suggested by the ratio of C_{30} αβ-hopane/*n*-C_{max} (range: 0.28–2.05, mean: 1.00) (Table 2, Fig. 7) (Carroll et al., 1992; Luo et al., 2018). Samples in this study contain moderate gammacerane/C_{30} hopane, ranging from 0.06 to 0.38, with a mean of 0.14 (Fig. 13C and Table 2). Steranes were detected in all samples, including C_{21}–C_{22} and C_{27}–C_{29} regular steranes (Fig. 7). The studied sample contain variable ratios of C_{27}/C_{29} regular steranes (0.28–0.84, mean: 0.49) and C_{28}/C_{29} regular steranes (0.46–1.38, mean: 0.81), respectively (Table 2, Fig. 8). With the content of C_{28} regular sterane gradually increasing, the peak patterns of regular sterane C_{27}, C_{28} and C_{29} vary from "√" shape to "/" shape and "Λ" shape (Fig. 7: sample A-5,sample A-7, sample A-12). The content of C_{28} regular sterane determines the distribution pattern of the peak of regular sterane (Fig. 7). It is the algae with high content of telalginite that contained relatively lower content of C_{28} regular sterane, but that was high in the lamalginite algae (Tables 1 and 2, Fig. 9c and d).

4.4. Inorganic geochemical characteristics

The elements B, V, Ni, and Cr are detected in all samples. The parameters of V/(V + Ni) ratio and V/Cr ratio were displayed in Table 2. The V/Cr ratios and V/(V + Ni) ratios were 1.72–3.73 and 0.65–0.81, averaging 2.55 and 0.71 respectively (Table 2). The boron content of the samples was between 89.4 and 316 ppm with an average of 164.08 (Table 2).

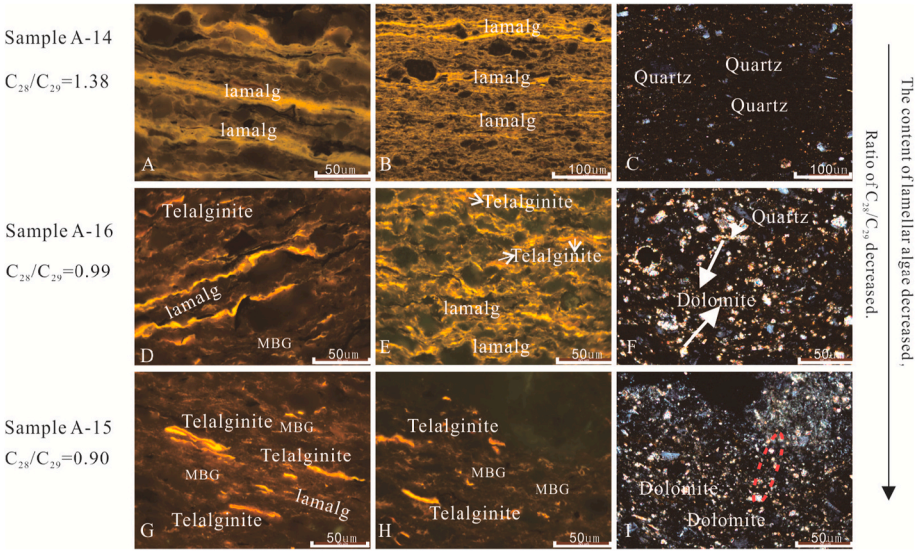

Fig. 5. Organic petrological and petrological of the samples with high ratio of C_{28}/C_{29} regular sterane. The observed samples were perpendicular to the bedding. A, D, and G are taken under oil immersion. A: brightly fluorescent lamalg with yellow color under fluorescence-inducing blue light (A-14, 3586.2m, polished section); B: Thin-section photograph showing lamalg with yellow color under fluorescence-inducing blue light (A-14, 3586.2m, thin-section); C: same field as (B) showing a lot of quartz and a little micritic dolomite under cross-polarized light; D: brightly fluorescent telalginite and lamalg with orange color under fluorescent light (A-16, 3595.4m depth, polished section); E: the microscopic photograph of thin-section, showing lamalg and telalginite with orange color under fluorescence-blue light (A-16, 3595.4m depth, thin-section); F: photograph of the same field as (E) showing secondary dolomite and quartz under cross-polarized light; G: brightly fluorescent lamalg, telalginite and MBG with orange color under fluorescent light (A-15, 3592.45m, polished section); H: Thin-section photograph showing the lamalg, telalginite and MBG with orange color under fluorescent light (A-15, 3592.45m, thin-section); I: Thin-section photograph of the same field as (H) showing dolomite and quartz under cross-polarized light. (For interpretation of the references to color in this figure legend, the reader is referred to the Web version of this article.)

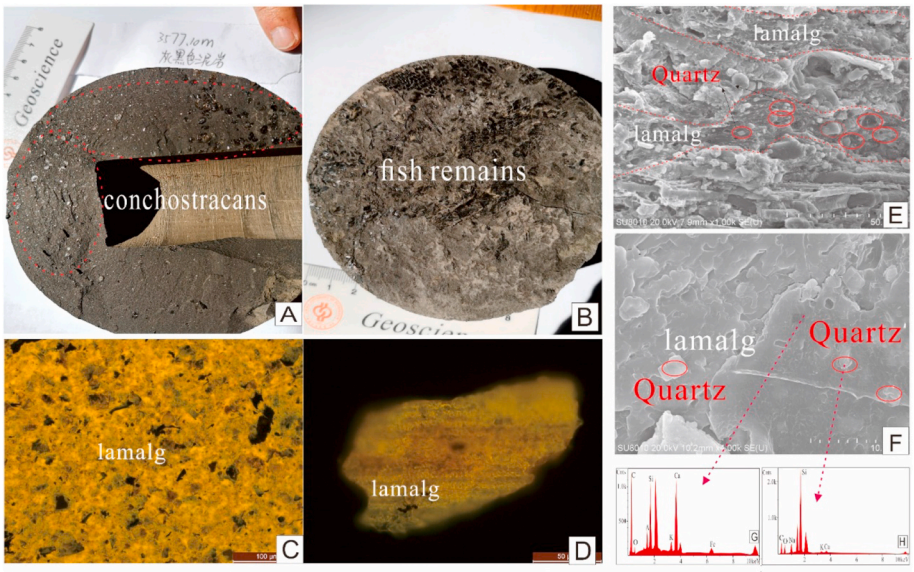

Fig. 6. A: Photograph of core with conchostracans, sample A-12, 3577.1m; B: Photo of core with fish remains, sample A-16, 3595.4m; C: Brightly fluorescent lamalg with green-yellow color under fluorescent light, the observed samples were all along parallel bedding planes, sample A-12, 3577.1m depth; D: photographs of lamalg under fluorescent light, kerogen of sample in 3577.1 m; E: SEM image of lamalg fossils, the observed samples were all along vertical bedding planes, sample A-12, 3577.1 m; F: SEM image of lamalg fossils, the observed samples were all along parallel bedding planes, sample A-12, 3577.1 m; G and H: The energy spectrum in F (the EDS of sampling point). (For interpretation of the references to color in this figure legend, the reader is referred to the Web version of this article.)

5. Discussion

5.1. Primary bio-precursors of source rock and biogenic source of C_{28} regular steranes

The bio-precursors in source rocks are mainly composed of aquatic algae, terrestrial higher plants, and bacteria (Volkman, 1986; Patterson, 1994; Nes and Venkatramesh, 1994; Volkman et al., 1998). In general, the sapropelinite plays a key role in improving the hydrocarbon generation potential of organic matter because it is dominated by aquatic algae and bacteria. Steranes represent biomarkers for algal eukaryotes and are preserved in sediments as steranes, whereas hopanes are typical biomarker for prokaryotic cyanophyte (Ourisson et al., 1979; Brocks et al., 1999; Summons et al., 1999). The shales are rich in organic matter (TOC: 1.47%–30.1%, mean = 7.51%) and show very good oil generation potential (HI: 358–823 mg HC/g TOC, mean = 659 mg HC/g TOC; Fig. 3B). Extremely high HI value indicate that the shales of the Lucaogou Formation are good to excellent potential source rocks. This also suggest that the primary organic components of the Lucaogou Formation are from aquatic algae, with relatively small contribution from terrigenous organic matter. This is consistent with the low contents of vitrinite and inertinite observed in the samples under the microscope. The organic components of the source rocks can be primarily divided into three types: telalginite, lamalginite, and mineral-bituminous groundmasses, with the dominance of the former two (Table 1). Due to the relatively heterogeneous nature of the source rocks, the contents of telalginite and lamalginite varies greatly with samples, which resulted from the different environments for the development of algae. The formation of mineral-bituminous groundmasses may be related to the action of bacteria (Stach et al., 1982; Wang et al., 1995). The carbon isotope of hopane of the organic matter in the Lucaogou Formation are as low as −61‰ (Xie et al., 2015), indicating the contribution of

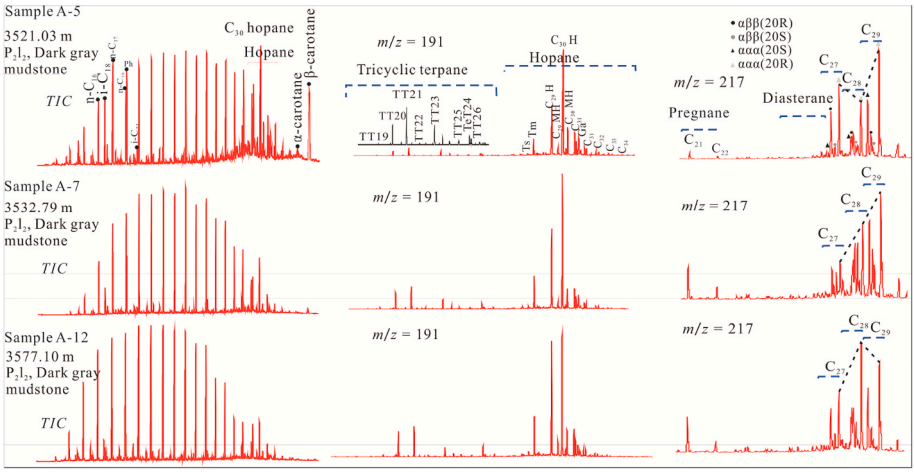

Fig. 7. Mass chromatograms of typical samples in this study.

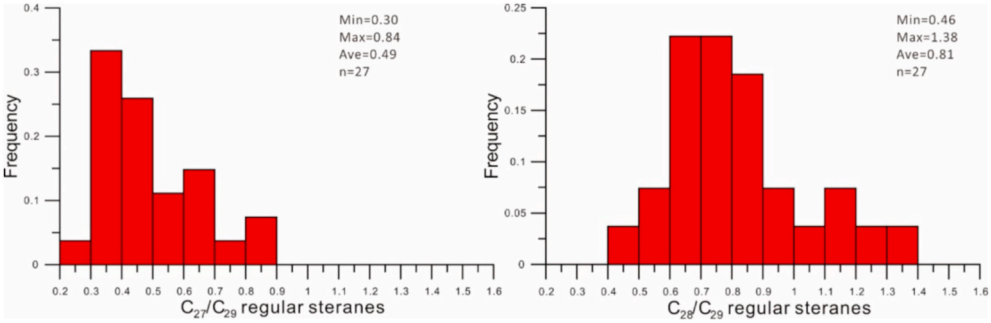

Fig. 8. Histograms of regular sterane C_{27}/C_{29} (left) and regular sterane C_{28}/C_{29} (right) ratios in the studied samples.

bacteria. Hopane dominance can be observed in the TIC spectra of the source rock, indicating bacteria contribution of, which is consistent with mineral-bituminous groundmasses observed in the samples (Table 1). By comparing with the ratios of C_{30} hopane/n-C_{max} in different samples, the relative contribution of bacteria in different samples can be roughly characterized (Fig. 7 and Table 2). Where the MBG is higher, C_{30} hopane/n-C_{max} >1 and predominance of telalginite (Fig. 9a). And MBG is 0%, C_{30} hopane/n-C_{max} < 1 and predominance of lamalginite (Tables 1 and 2, Fig. 9b). It indicates that the environment for the development of bacteria and lamalginite were consistent.

At present, there are several biogenic sources of steroids including algae terrestrial plants, fungi and animals (Volkman, 1986; Patterson, 1994; Nes and Venkatramesh, 1994; Volkman et al., 1998; Volkman, 2003, 2005), but that from terrestrial plants is in less input to the sedimentary environment, the algae is considered to be the primary producer of sterane. The study on algae have shown that different types of algae tend to have multiple sterols, but vary greatly in the contents, thereby to provide a possibility to trace the precursor of algae (Volkman, 1986; Patterson, 1994; Nes and Venkatramesh, 1994; Volkman et al., 1994, 1998). In Figs. 4 and 7, it can be found that Sample A-5 was dominated by telalginite and its corresponding C_{28} regular sterane was relatively low, and the relative content of regular sterane was characterized by the distribution pattern of $C_{29} > C_{27} > C_{28}$. Both the telalginite and lamalginite were developed in Sample A-7, the content of C_{28} sterane was correspondingly increased, and the relative content of regular steranes was in the distribution pattern of $C_{29} > C_{28} > C_{27}$ in the spectrum. The Sample A-12 was dominated by lamalginite from organic petrological observation and statistics, but it contained the highest content of C_{28} sterane and regular sterane and the distribution pattern of relative content of $C_{28} > C_{29} > C_{27}$. At the same time, as the content of lamalginite increases, the ratio of C_{28}/C_{29} was increased as well (Figs. 5 and 12a). The relationship between the percentage of C_{28} regular sterane content and the content of telalginite and lamalginite can also be observed. That is, the percentage of C_{28} regular sterane ($C_{28}/(C_{27} + C_{28} + C_{29})$ regular sterane) has a good positive correlation with lamalginite and a negative correlation with telalginite (Fig. 9, Table 1), indicating that the primary source of C_{28} sterane is lamalginite.

Cook and Sherwood (1991) divided lamalginite-rich oil shales into two categories including marosite and lacosite. The marosite rocks are formed only in marine saline environments and the lacosite are formed in a lacustrine fresh-brackish or brackish water environment. Lacosite can be further divided into the rundle type and the Green River type. The rundle type was usually characterized by the morphology of short laminae, and the main algae sources are chlorophyta and dinoflagellates. The Green River type was usually characterized by the morphology of long Laminae, and it is mainly sourced from cyanobacteria biogenically (Fig. 10). As can be seen from Fig. 4G, Fig. 5B, C, D, and E and Fig. 6E and F, the lamalginite of Lucaogou Formation in the Jimusaer Sag extend very long and form a lamellar superposition, which is similar to the Green River type. Moreover, the content of C_{28} regular sterane in the shale of the Green River Formation also demonstrated a significant predominance (Fig. 11) (Katz, 1995). In addition, compound specific isotope of the Green River shale has been analyzed (Collister, 1992) with almost same compound specific isotope composition of kerogen and compound C_{28} sterane, which just has explained the algal origin of C_{28} sterane. In combination with morphological and biomarker characteristics, the lamalginite in the Lucaogou Formation should be derived from cyanobacteria which is the same as the oil shale of the Green River Formation. Under the microscopic observation of samples, there are a large number of fine quartz particles between the lamalginite sheets in the Lucaogou Formation (Fig. 6E and F). According to the research of modern cyanobacteria, high concentration of extracellular

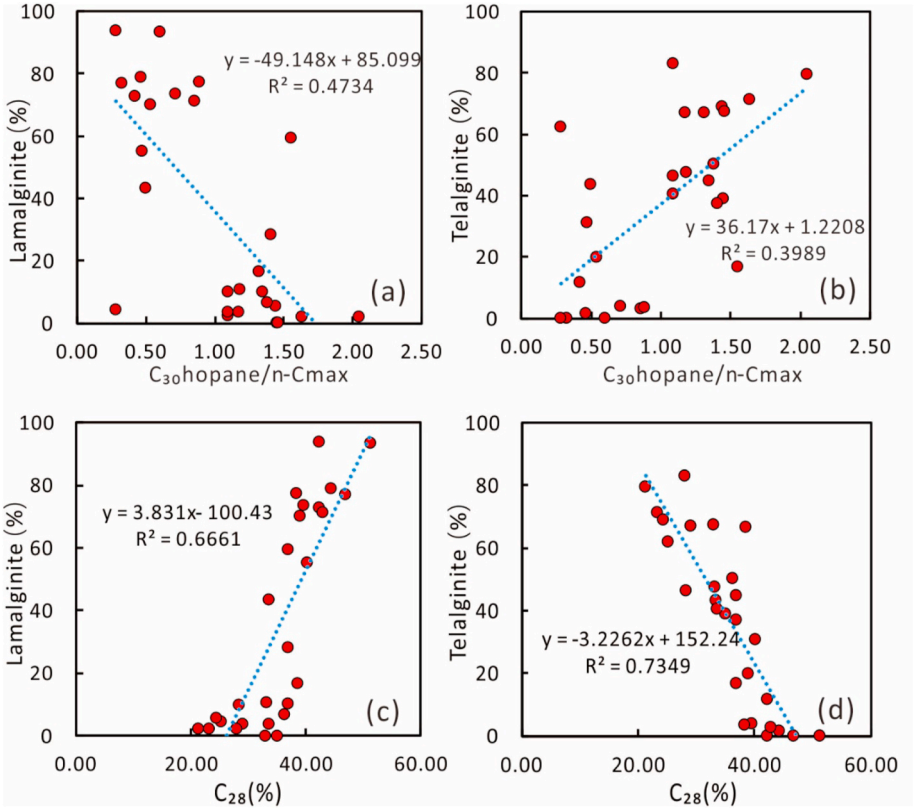

Fig. 9. Cross plots of C_{30}hopane/n-Cmax versus Lamalginite(%) (a), C_{30}hopane/n-Cmax versus Telaginite(%) (b), C_{28}(%) versus Lamalginite(%) (c), and C_{28}(%) versus Telalginite (%) (d) of the Lucaogou Formation shale samples. Note: C_{28}%: $C_{28}/(C_{27}+C_{28}+C_{29})$ regular sterane.

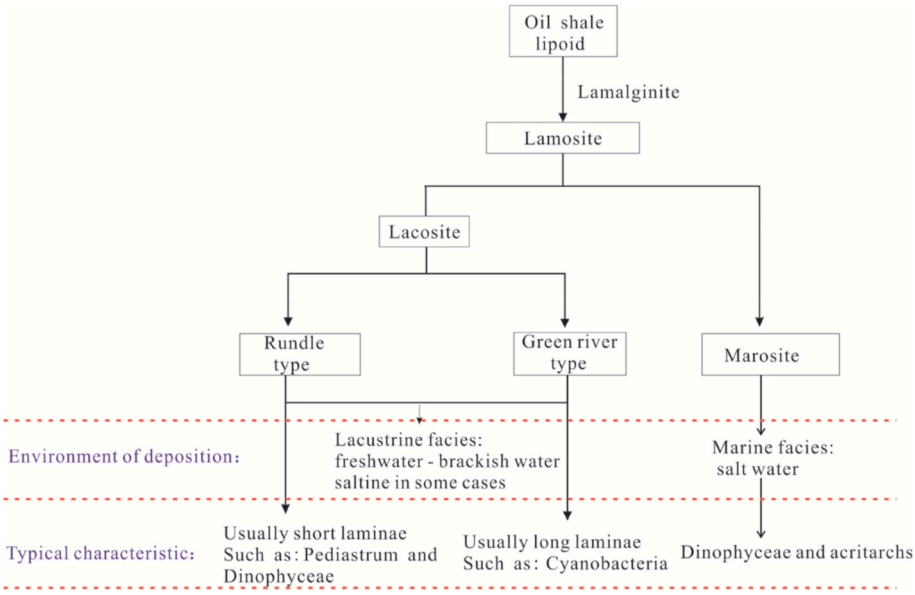

Fig. 10. Classification of lamalginite from oil shale (Cook and Sherwood, 1991).

polymeric substances (EPS) (Hu, 2011) can frequently be generated by large amounts of algae cells when there is the progradation of cyanobacteria (Hu, 2011; Pierre et al., 2013), it is the characterized by high viscosity and can agglutinate several to several hundreds of cyanobacteria cells with a diameter of 4–6 μm, resulting the formation of an amorphous group of cyanobacteria with a maximum diameter of 1000 μm (Sun et al., 2014). The extracellular polymer substance of cyanobacteria can also adsorb large quantities of small quartz particles and the minerals will precipitate and form algal mats as the adsorption increases (Cameron et al., 1985; Stal et al., 1985). Moreover, modern cyanobacteria cultured in glucose can produce large amounts of ergosterol (1033.3 μg/g), a precursor to ergosterane (C_{28} sterane) (Fagundes et al., 2019). It further confirmed that the lamalginite are sourced from cyanobacteria. The Green river shale and Lucaogou Formation shale shared similarities in the biomarkers and organic petrological characteristics, indicating cognate hydrocarbon-generating material in saline lacustrine,

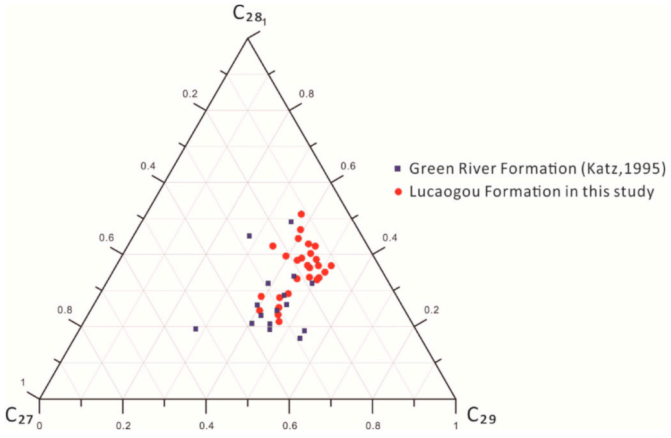

Fig. 11. Ternary plot showing relative abundance of the C_{27}, C_{28} and C_{29} regular steranes from the Green River Formation (Katz, 1995) and the Lucaogou Formation shale samples in this study. (For interpretation of the references to color in this figure legend, the reader is referred to the Web version of this article.)

for instance, similar biomarkers characteristics were also observed in the Fengcheng Formation in the Junggar Basin (Cao et al., 2020).

5.2. Environment for the development of different biogenic source

In the process of core observation, it was usually found that the lamalginite samples contained some conchostracans and fish remains (bones; Table 1, Fig. 6A and B). These two species were mainly adaptable to fresh or brackish water (Martill et al., 2011; Berrell et al., 2014; Lara et al., 2017), indicating that lamalginite(cyanobacteria) developed in the fresh-brackish water depositional environment.

The mineralogical composition of rocks can be used to deduce the paleo-sedimentary environment, and its carbonate content (Milliman, 1993; Flügel, 2010). A large amount of micritic dolomite can be observed in the source rock samples dominated by telalginite (green algae) (Fig. 4C). This indicate a highly saline depositional environment (Brand and Veizer, 1981; Kaufman et al., 1991). In the source rocks dominated by lamalginite (cyanobacteria), there is trace to no carbonates, but a large amount of fine-grained quartz (Figs. 4I, 5C and 6F), indicating low salinity water column. However, when lamalginite and telalginite are both developed in the shale, the quartz and the carbonate are relatively well developed (Fig. 4F), indicating that the environment in which they formed was a transitional environment.

The ratio of C_{28}/C_{29} regular sterane has a correlate positively with percent lamalginite algae (Fig. 12a), and a negative correlation with the percent telalginite algae (Fig. 12b), indicating that the Lamalginite is the source of C_{28} regular sterane and the C_{29} regular sterane is biogenically from the telalginite. We thought the regular sterane C_{28}/C_{29} ratio greater than 0.9 indicated that the source rocks were dominated by lamalginite (cyanobacteria). The regular sterane ratio $C_{28}/C_{29} < 0.7$ indicated that the source rocks were dominated by telalginite (green algae) (Fig. 12). The regular C_{28}/C_{29} sterane ratio of 0.7–0.9, indicate both types of algae are developed in the source rock. From Fig. 13A and B, there was a good correlation between isoparaffins. However, in the source rocks dominated by lamalginite and telalginite, respectively, the correlation coefficient between isoparaffins (lamalginite: $R^2 = 0.9833$ (i-C_{21}/n-C_{19} versus Ph/n-C_{18}), $R^2 = 0.9819$ (Pr/n-C_{17} ratio versus Ph/n-C_{18}); telalginite: $R^2 = 0.8792$ (i-C_{21}/n-C_{19} versus Ph/n-C_{18}), $R^2 = 0.8716$ (Pr/n-C_{17} ratio versus Ph/n-C_{18}) was significantly better than the source rock samples where both algae were developed ($R^2 = 0.5109$ (i-C_{21}/n-C_{19} versus Ph/n-C_{18}), $R^2 = 0.5109$ (Pr/n-C_{17} ratio versus Ph/n-C_{18}). This is because environmental parameters are more stable and uniform in the development of monotonous specie of algae. The crossplot of Pr/n-C_{17} versus Ph/n-C_{18} is frequently used to identify the organic matter input and depositional conditions of source rocks (Connan and Cas Sou, 1980; Shanmugam, 1985). Fig. 13B shows that the Lucaogou Formation shale was deposited in the transitional to reducing environment. Pristane (Pr) and phytane (Ph) are typically the most important acyclic isoprenoids (Powell and McKirdy, 1973), which reflect environmental conditions during deposition (Didyk et al., 1978; Moldowan et al., 1986; Peters et al., 2005). From Fig. 13C, it can be seen that they were mainly formed in the anoxic to dysoxic/suboxic lacustrine depositional environment. The content of phytane, i-C_{21}, gammacerane and β-carotane can reflceted the paleo-salinity during deposition. The higher the salinity is, the higher the higher the content of phytane, i-C_{21}, gammacerane and β-carotane is (Connan and Cas Sou, 1980; Hall and Douglas, 1981; Shanmugam, 1985; Jiang and Flower, 1986; Moldowan, 1985; Peters and Moldowan, 1993). Also, gammacerane is known to reflect water column stratification (e.g. Sinninghe Damsté et al., 1995). The abundance of phytane, i-C_{21}, gammacerane and β-carotane as proven by the ratios of Ph/n-C_{18}, i-C_{21}/n-C_{19}, gammacerane index (Gammacerane/C_{30} Hopane) and β-carotane/n-C_{max} (Table 2). As can be seen from Fig. 13A, B and D, the biomarker parameters of Ph/n-C_{18}, i-C_{21}/n-C_{19} and β-carotane/n-C_{max} ratios in rock samples with the development of telalginite (green algae) were the highest, and the correlation ratio parameters of rock samples with the development of lamalginite (cyanobacteria) were the lowest. The correlation ratio parameters of samples with the development of both types of algae were located in the middle. This shows that lamalginite (cyanobacteria) was developed when the salinity of water was low and telalginite (green algae) was developed when the salinity of water was high. The gammacerane index is no significant differences between the samples with development of lamalginite (cyanobacteria) and the samples with development of telalginite (green algae) (Fig. 13C), but Fig. 13C showed that the shale samples of Lucaogou formation were mainly deposited in the depositional environment of normal salinity–higher salinity with weakly stratified water

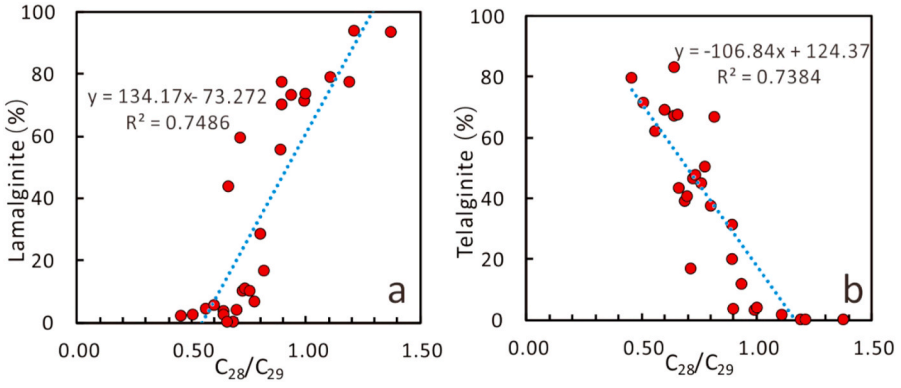

Fig. 12. Cross plots of C_{28}/C_{29} ratios versus (a) Lamalginite (%) and (b) Telalginite (%) of the Lucaogou Formation shale samples.

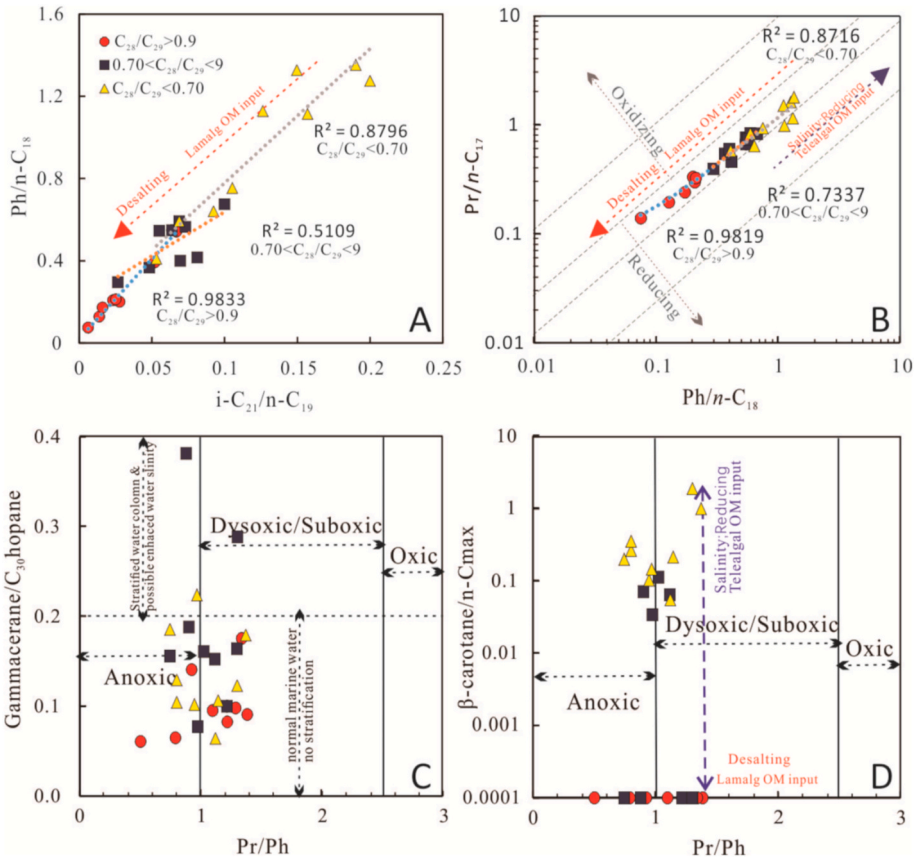

Fig. 13. Cross plots of *i*-C_{21}/n-C_{19} versus Ph/*n*-C_{18} ratios (A), Pr/*n*-C_{17} ratio versus Ph/*n*-C_{18} ratio (B), Pr/Ph ratio versus gammacerane/C_{30}hopane ratio (C) and Pr/Ph ratio versus *β*-carotane/*n*-C_{max} ratios (D) of the Lucaogou Formation shale samples. C_{28}/C_{29}:C_{28}/C_{29} regular sterane. B: after Connan and Cas Sou.1980; C: after Song et al., 2016

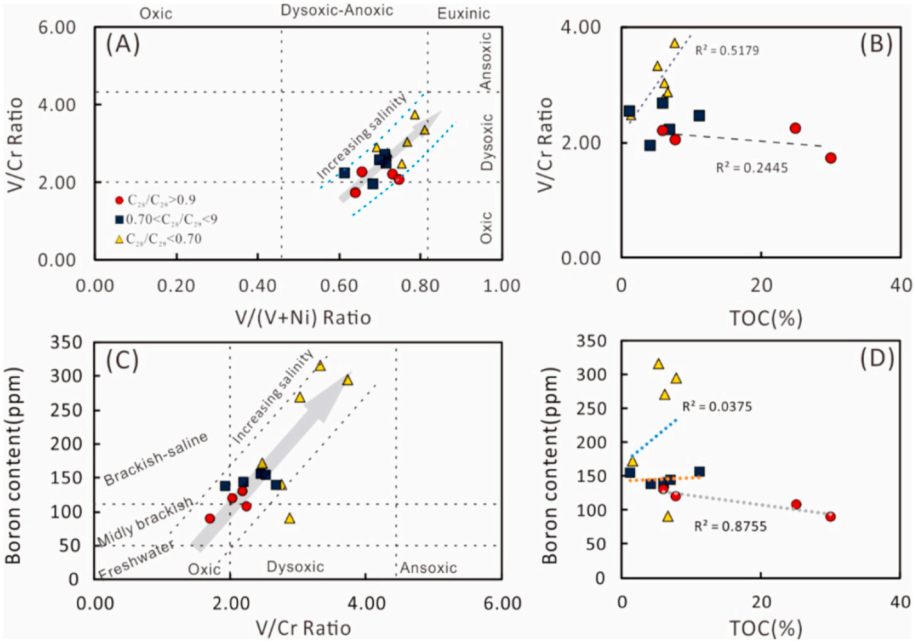

Fig. 14. Cross plots of V/(V + Ni) ratio versus V/Cr ratios (A), TOC content versus V/Cr ratio (B), V/Cr ratio versus Boron content (C) and TOC content versus Boron content (D) of the Lucaogou Formation shale samples. A: according to Wingnall and Hatch (1994) and Jones and Manning (1994); C: according to Banerjee and Goodarzi (1990) and Jones and Manning (1994).

column.

The ratio of trace elements V/Cr, V/(V + Ni) and boron element content to characterize the redox conditions and salinity of sedimentary water (Potter et al., 1963; Walker and Price, 1963; Campbell and Williams, 1965; Hatch and Leventhal, 1992; Jones and Manning, 1994; Rimmer, 2004). The sedimentary environment index of V/Cr ratio is given by Jones (1994) with V/Cr ratio less than 2.00 indicating an oxidizing environment, V/Cr ratio greater than 4.25 indicating anoxic (reducing) environment, the interval values indicating a transitional environment from secondary oxidation to secondary reduction. The trace elements V and Ni were also used by Wingnall and Hatch(1994) to identify the sedimentary environment, V/(V + Ni) ratio less than 0.60 indicates that the ancient ocean water body is a weakly stratified and oxidized. The V/(V + Ni) index in the range of 0.60–0.84 indicates an oxygen-deficient environment; V/(V + Ni) greater than 0.84 indicates an euxinic facies reducing environment and the paleo-ocean water body is strongly stratified. The boron content less than 50 ppm, 50–110 ppm and >100 ppm can represent fresh water, brackish water and brackish water-salt water environment correspondingly (Banerjee and Goodarzi, 1990). In the paper, the V/Cr ratios and V/(V + Ni) ratios were 1.72–3.73 and 0.65–0.81, averaging 2.55 and 0.71 respectively (Table 2). It indicates that the source rocks of the Lucaogou Formation are mainly deposited under sub-redox conditions (Fig. 14a), which is consistent with the results of the biomarker compound parameter Pr/Ph. The boron content of the samples was between 89.4 and 316 ppm with an average of 164.08 (Table 2). The salinity index indicates that the Lucaogou Formation is mainly deposited in the brackish-saline water environment (Fig. 14c). The changes in the abovementioned parameters also indicate the slight changes in the sedimentary environment during the deposition of source rocks. The samples dominated by telalginite (C_{28}/C_{29} < 0.7) have relatively high V/Cr ratio and boron content. Samples dominated by lamalginite (C_{28}/C_{29} > 0.9) have lower V/Cr ratio and boron content. Samples with both telalginite and lamalginite developed in the source rock showed parameters between the abovementioned two end members (Fig. 14). The relationship between the organic carbon content and the V/Cr ratio and boron content further indicates that the telalginite is developed in a water environment with higher salinity and stronger reducibility. However, the lamalginite algae are more developed in water body with lower salinity (Fig. 14b and d).

5.3. Potential and conversion of hydrocarbon generation

A direct correlation has been reported between rock pyrolysis and hydrocarbon generation potential (Peter and Cassa, 1994; Jarvie, 2001). The samples were mainly lacustrine mudstone, with high organic matter content. The average TOC and S_2 are 7.51% and 51.93 mg HC/g rock, respectively (Table 1). TOC and S_2 values indicate that these mudstones are mainly good to excellent source rocks with good to excellent hydrocarbon-generating potential (Fig. 15A). Rock-Eval parameter HI is used to evaluate the organic matter type in source rocks (Waples, 1985). These mudstones are dominated by Type II and I kerogen (Fig. 15B). The HI of the samples dominated by telalginite is slightly lower than that of the lamalginite-dominated samples (Fig. 15C). This indicates that the two types of algae have different hydrocarbon generation characteristics. This is due to the fact that the original hydrocarbon generation potential of telalginite is lower than that of lamalginite, or the telalginite generates hydrocarbons earlier than lamalginite, resulting in the lower HI than lamalginite under the same thermal maturity level, a

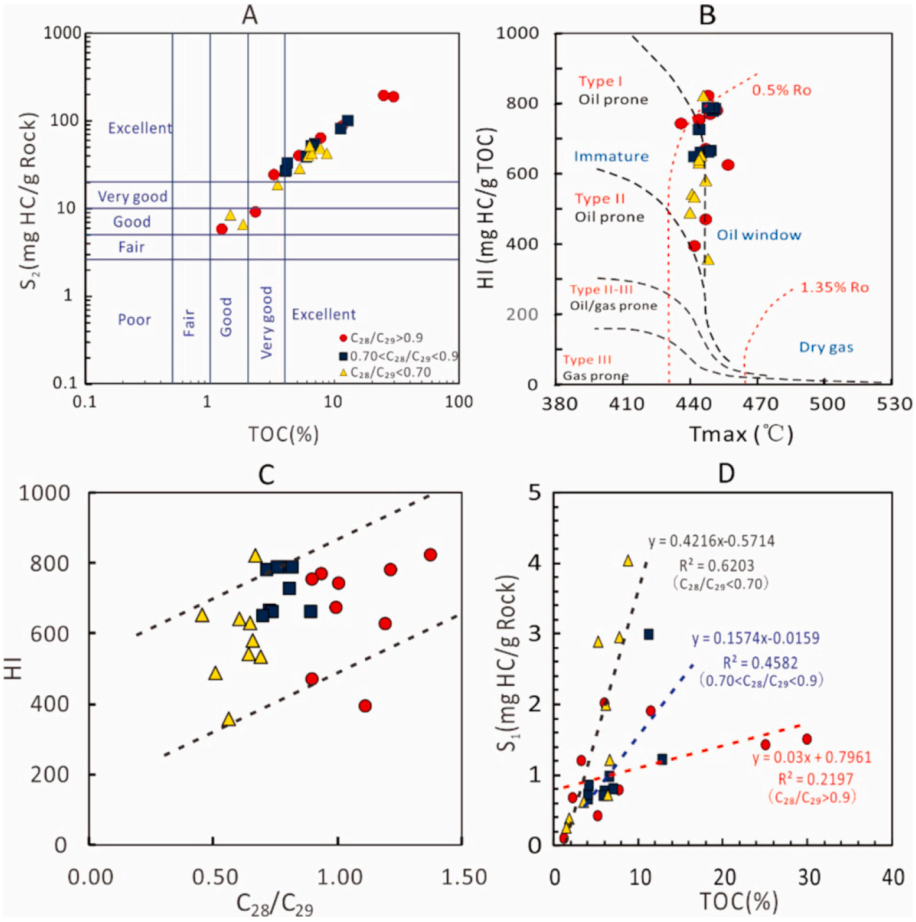

Fig. 15. Cross plots of TOC versus S_2 ratio (A), Tmax versus HI (B), C_{28}/C_{29} versus HI (C) and TOC versus S_1 (D) of the Lucaogou Formation shale samples. C_{28}/C_{29}: C_{28}/C_{29} regular sterane. A: after Peters and Cassa (1994); B: after Mukhopadhyay et al. (1995)..

phenomenon illustrated on Fig. 15D. It can be seen from Fig. 15D that TOC and S_1 were linearly correlated. The slope of samples with telalginite: $K_{C28/C29<0.7} = 0.4216 >$ the slope of samples with both types of algae: $K_{0.7<C28/C29<0.9} = 0.1574 >$ the slope of samples developed by lamalginite: $K_{C28/C29>0.9} = 0.03$. The higher K is, the easier it is to generate hydrocarbons. The maceral observations were correspondingly also consistent, and the fluorescence of the lamalginite in the sample was yellowish-green (Figs. 4G and 5A), indicating that the lamalginite are at a lower hydrocarbon-generating stage. The fluorescence of telalginite is orange-brown (Figs. 4A and 5G), indicating that telalginite was in a higher hydrocarbon-generating stage. In other words, in the lower thermal evolution stage of the Lucaogou Formation source rock, the telalginite has higher hydrocarbon-generating conversion rate than the lamalginite.

6. Conclusion

Based on the organic petrology observation, lithology observation and biomarker analyses of shale samples of the Lucaogou Formation in the Jimusaer Sag, Junggar Basin, northwest China, it was determined that the precursor composition in the source rock was three types: telalginite, lamalginite, and mineral-bituminous groundmasses, with the dominance of the former two.

Based on organic petrology, molecular geochemical and geochemistry of element analyses among different samples, the biogenic origin of C_{28} sterane was identified as lamalginite (cyanobacteria). Combined with the analyses of petrology and molecular geochemistry, the shale in Lucaogou Formation were mainly deposited in the depositional environment of normal salinity–higher salinity with weakly stratified water column. And it is clarified that the lamalginite (cyanobacteria) is more developed when the salinity is low and the telalginite (green algae) is more developed when the salinity is high.

Based on geochemical parameters and fluorescence of different algae, both the telalginite and lamalginite have good hydrocarbon-generating potential, but in the lower thermal evolution stage of the Lucaogou Formation source rock, the lamalginite has lower hydrocarbon-generating rate than the telalginite.

Credit author statement

Liu Shiju: Data curation, Writing-original draft. Gang Gao: Conceptualization, Methodology, Supervision. Jun Jin: Data curation, Investigatiion. Wenzhe Gang: Methodology, Supervision. Baoli Xiang: Data Curation.

Declaration of competing interest

The authors declare that they have no known competing financial interests or personal relationships that could have appeared to influence the work reported in this paper.

Acknowledgements

We would like to thank Xinjiang Oilfield Company for allowing the publication of the manuscript, and in particular, they have provided part of the geochemistry data of shales and stratigraphic framework for us.

References

Bai, H., Pang, X., Kuang, L., Pang, H., Wang, X., Jia, X., Zhou, L., Hu, T., 2016. Hydrocarbon expulsion potential of source rocks and its influence on the distribution of lacustrine tight oil reservoir, Middle Permian Lucaogou Formation, Jimsar Sag, Junggar Basin, Northwest China. J. Petrol. Sci. Eng. https://doi.org/10.1016/j.petrol.2016.09.053.

Banerjee, I., Goodarzi, F., 1990. Paleoenvironment and sulfur-boron contents of the mannville (lower cretaceous) coals of southern alberta. Canada. Sediment. Geol. 67, 297–310. https://doi.org/10.1016/0037-0738(90)90040-Z.

Berrell, R.W., Alvarado-Ortega, J., Yabumoto, Y., Salisbury, S.W., 2014. The first record of the ichthyodectiform fish Cladocyclus from eastern Gondwana: a new species from the Lower Cretaceous of Queensland, Australia. Acta Palaeontol. Pol. 59 (4), 903–920.

Brand, U., Veizer, J., 1981. Chemical diagenesis of a multicomponent carbonate system-2, stable isotopes. J. Sediment. Petrol. 51, 987–997. https://doi.org/10.1306/212F7DF6-2B24-11D7-8648000102C1865D.

Brocks, P., Rohjans, D., Scholz-Böttcher, Barbara M., Rullkötter, Jürgen, 1999. Molecular composition of organic matter in the sediment of a mussel bee as an indicator of ecological variations. Mar. Biodivers. 29 (5 Suppl), 45–50. https://doi.org/10.1007/BF03043119.

Cameron, B., Cameron, D., Jones, J.R., 1985. Modern algal mats in intertidal and supratidal quartz sands, northeastern Mas- sachusetts, USA. In: Curren, H.A. (Ed.), Biogenic Structures: Their Use in Interpreting Depositional Environments, vol. 35. Society of Economic Paleontologists and Mineralogists. SEPM special publication, Tulsa, OK, pp. 211–235.

Campbell, F.A., Williams, G.D., 1965. Chemical composition of shales of mannville group (lower cretaceous) of central alberta, Canada. Am. Assoc. Petrol. Geol. Bull. 49, 81–87. https://doi.org/10.1306/A66334EA-16C0-11D7-8645000102C1865D.

Cao, Jian, Xia, Liuwei, Wang, Tingting, Zhi, Dongming, et al., 2020. An alkaline lacustrine in the Late Paleozoic Ice Age (LPIA): a review and new insights into paleoenvironment and petroleum geology. Earth Sci. Rev. 202, 103091. https://doi.org/10.1016/j.earscirev.2020.103091, 2020.

Carroll, A.R., 1998. Upper permian lacustrine organic facies evolution, southern Junggar Basin NW China. Org. Geochem. 28, 649–667. https://doi.org/10.1016/S0146-6380(98)00040-0.

Connan, L., Cas Sou, A.M., 1980. Properties of gases and petroleum liquids derived from terrestrial kerogen at various maturation levels. Geochimica & Cosmchimica Acta 44, 1–23. https://doi.org/10.1016/0016-7037(80)90173-8.

Cook, A.C., Sherwood, N.R., 1991. Classification of oil shales, coals and other organic-rich rocks. Org. Geochem. https://doi.org/10.1016/0146-6380(91)90079-Y.

Didyk, B.M., Simoneit, B.R.T., Brassel, S.C., Eglinton, G., 1978. Organic geochemical indicators of paleoenvironmental conditions of sedimentation. Nature 272, 216–222.

Espitalié, J., Deroo, G., Marquis, F., 1985. La pyrolysis Rock-Eval et ses applications. Rev. Inst. Fr. Petrol 40, 755–784. https://doi.org/10.2516/ogst:1985045.

Fagundes, M.B., Falk, R.B., Facchi, M.M.X., et al., 2019. Insights in cyanobacteria lipidomics: a sterols characterization from Phormidium autumnale biomass in heterotrophic cultivation. Food Res. Int. https://doi.org/10.1016/j.foodres.2018.10.060.

Fang, Shihu, Xu, Huaimin, Song, Yan, et al., 2005. Characteristics and evolution of the composite petroleum system in Jimsaer Depression, eastern Junggar Basin. Acta Geosci. Sin. 26 (3), 259–264. https://doi.org/10.3975/cagsb.2005.03.11.

Flügel, Erik, 2010. Microfacies of carbonate rocks analysis. Interpretation and Application. https://doi.org/10.1007/978-3-662-08726-8.

Frimmel, H.E., 2008. An evaporitic facies in Neoproterozoic post-glacial carbonates: the Gifberg Group, South Africa. Gondwana Res. 13, 453–468. https://doi.org/10.1016/j.gr.2007.05.002.

Gao, G., Zhang, W., Xiang, B., Liu, G., Ren, J., 2016. Geochemistry characteristics and hydrocarbon–generating potential of lacustrine source rock in Lucaogou Formation of the Jimusaer Sag, Junggar Basin. J. Petrol. Sci. Eng. 145, 168–182. https://doi.org/10.1016/j.petrol.2016.03.023.

Grantham, P.J., Wakefield, L.L., 1988. Variations in the sterane carbon number distributions of marine source rock derived crude oils through geological times. Org. Geochem. 12, 61–77. https://doi.org/10.1016/j.palaeo.2006.03.050.

Hackley, P.C., Fishman, N., Wu, T., Baugher, G., 2016. Organic petrology and geochemistry of mudrocks from the lacustrine Lucaogou Formation, Santanghu Basin, northwest China: application to lake basin evolution. Int. J. Coal Geol. 168, 20–34. https://doi.org/10.1016/j.coal.2016.05.011.

Hall, P.B., Douglas, A.G., 1981. The distribution of cyclic alkanes in two lacstrine deposits. Advances in Organic Geochemistry, 576–587.

Hatch, J.R., Leventhal, J.S., 1992. Relationship between inferred redox potential of the depositional environment and geochemistry of the upper pennsylvanian (missourian) Stark shale member of the dennis limestone, wabaunsee county, Kansas, USA. Chem. Geol. 99, 65–82. https://doi.org/10.1016/0009-2541(92)90031-Y.

Horsfield, B., Curry, D.J., Bohacs, K., et al., 1994. Organic geochemistry of freshwater and alkaline lacustrine sediments in the Green River Formation of the Washakie Basin, Wyoming, U.S.A. Org. Geochem. 22 (3–5) https://doi.org/10.1016/0146-6380(94)90117-1, 0-440.

Hu, Hongjun, 2011. The Biology of Cyanobacteria. Science Press, Beijing.

Huang, W.Y., Meinschein, W.G., 1979. Sterols as ecological indicators. Geochimica et Cocmochimica Acta 43, 739–745. https://doi.org/10.1016/0016-7037(79)90257-6.

Hutton, Adrian C., 1987. Petrographic classification of oil shales. Int. J. Coal Geol. 203–231. https://doi.org/10.1016/0166-5162(87)90032-2.

Jarvie, D.M.H.G., 2001. Detection of pay zones and pay quality, gulf of mexico: application of geochemical techniques. AAPG Bull. 85 https://doi.org/10.1306/8626CED3-173B-11D7-8645000102C1865D.

Jiang, Z.S., Flower, M.G., 1986. Carotenoid-derived alkanes in oils from northwestern China. Org. Geochem. 10, 831–839. https://doi.org/10.1016/s0146-6380(86)80020-1.

Jones, B., Manning, D.A.C., 1994. Comparison of geochemical indices used for the interpretation of palaeoredox conditions in ancient mudstones. Chem. Geol. 111, 111–129. https://doi.org/10.1016/0009-2541(94)90085-x.

Katz, B.J., 1995. The green river shale: an eocene carbonate lacustrine source rock. https://doi.org/10.1007/978-3-642-78911-3_16.

Kaufman, A.J., Hayes, J.M., Knoll, A.H., Germs, G.J.B., 1991. Isotopic compositions of carbonates and organic carbon from upper Proterozoic successions in Namibia, stratigraphic variation and the effects of diagenesis and metamorphism. Precambrian Res. 49, 301–327. https://doi.org/10.1016/0301-9268(91)90039-D.

Kuang, L., Tang, Y., Lei, D., Chang, Q., Ouyang, M., Hou, L., Liu, D., 2012. Formation conditions and exploration potential of tight oil in the Permian saline lacustrine dolomitic rock, Junggar Basin, NW China. Petrol. Explor. Dev. 39 (6), 700–711. DOI: CNKI:SUN:SKYK.0.2012-06-004.

Lara, M.B., Cariglino, B., Zavattieri, A.M., 2017. Palaeoenvironmental interpretation of an Upper Triassic deposit in southwestern Gondwana (Argentina) based on an insect fauna, plant assemblage, and their interactions. Palaeogeogr. Palaeoclimatol. Palaeoecol. https://doi.org/10.1016/j.palaeo.2017.03.029. S0031018216308938. DOI.

Liu, Bo, Bechtel, Achim, Sachsenhofer, Reinhard F., Gross, Doris, Gratzer, Reinhard, Chen, Xuan, 2017. Depositional environment of oil shale within the second member of Permian Lucaogou Formation in the Santanghu Basin, Northwest China. Int. J. Coal Geol. 175, 10–25. https://doi.org/10.1016/j.coal.2017.03.011.

Luo, Q., Gong, L., Qu, Y., Zhang, K., Zhang, G., Wang, S., 2018. The tight oil potential of the Lucaogou Formation from the southern Junggar Basin, China. Fuel 234, 858–871. https://doi.org/10.1016/j.fuel.2018.07.002.

Martill, D.M., Ibrahim, N., Brito, P.M., Baider, L., Zhouri, S., Loveridge, R., Naish, D., Hing, R., 2011. A new Plattenkalk Konservat Lagerstatte in the Upper Cretaceous ϵ of Gara Sbaa, south-eastern Morocco. Cretac. Res. 32 (4), 433–446. https://doi.org/10.1016/j.cretres.2011.01.005.

Meng, Qingtao, Liu, Zhaojun, Liu, Rong, Sun, Pingchang, Hu, Fei, Zhang, Jing, 2011. Comparision on the Characteristics of Biomarkers of Oil Shale between Huadian Formation in Huadian Basin and Green River Formation in Uinta Basin of Western United States. Journal of Jilin University (Earth Science Edition 41, P391–399. https://doi.org/10.13278/j.cnki.jjuese.2011.02.028.

Milliman, J.D., 1993. Production and accumulation of calcium carbonate in the ocean: budget of a nonsteady state. Global Biogeochem. Cycles 7 (4). https://doi.org/10.1029/93gb02524, 927-0.

Moldowan, J.M., 1985. Organic geochemistry division of the geochemical society: alfred e. treibs award introduction of wolfgang k. scifert for the alfred e. treibs award 1984. Geochem. Cosmochim. Acta 49 (7), 1671–1672. https://doi.org/10.1016/0016-7037(85)90276-5.

Moldowan, J.M., Sundararaman, P., Schoell, M., 1986. Sensitivity of biomarker properties to depositional environment and/or source input in the Lower Toarcian of S.W. Germany. Org. Geochem. 10, 915–926. https://doi.org/10.1016/S0146-6380(86)80029-8.

Mukhopadhyay, P.K., Wade, J.A., Kruge, M.A., 1995. Organic facies and maturation of Cretaceous/Jurassic rocks and possible oil-source rock correlation based on pyrolysis of asphaltenes, Scotian basin. Canada. Org. Geochem. 22, 85–104. https://doi.org/10.1016/0146-6380(95)90010-1.

Nes, W.D., Venkatramesh, M., 1994. Molecular asymmetry and sterol evolution. In: Nes, W.D. (Ed.), Isopentenoids and Other Natural Products — Evolution and Function, vol. 562. ACS Symposium Series, pp. 55–89. https://doi.org/10.1021/bk-1994-0562.ch004.

Ourisson, G., Albrecht, Pierre, Rohmer, M., 1979. The hopanoids: palaeochemistry and biochemistry of a group of natural products. Pure Appl. Chem. 709–729. https://doi.org/10.1351/pac197951040709.

Patterson, G.W., 1994. Phylogenetic distribution of sterols. In: Nes, W.D. (Ed.), Isopentenoids and Other Natural Products—Evolution and Function, vol. 562. ACS Symposium Series, pp. 90–108.

Peters, K.E., 1986. Guidelines for evaluating petroleum source using programmed pyrolysis. AAPG Bull. 70, 318–329. https://doi.org/10.1306/94885688-1704-11D7-8645000102C1865D.

Peters, K.E., Cassa, M.R., 1994. Applied source rock geochemistry. In: Magoon, L.B., Dow, W.G. (Eds.), The Petroleum System – from Source to Trap. American Association of Petroleum Geologists, Tulsa, OK, pp. 3–117.

Peters, K.E., Moldowan, J.M., 1993. The Biomarker Guide: Interpreting Molecular Fossils in Petroleum and Ancient Sediments. Prentice–Hall, Englewood Cliffs, N. J. DOI: https://doi.org/.

Peters, K.E., Walters, C.C., Moldowan, J.M., 2005. The Biomarker Guide. Cambridge University Press, Cambridge. https://doi.org/10.1017/CBO9780511524868.

Potter, P.E., Shimp, N.F., Witters, J., 1963. Trace elements in marine and fresh-water argillaceous sediments. Geochem. Cosmochim. Acta 27, 669–694. https://doi.org/10.1016/0016-7037(63)90019-X.

Powell, T.G., McKirdy, D.M., 1973. Relationship between ratio of pristane to phytane, crude oil composition and geological environment in Australia. Nature 243, 37–39. https://doi.org/10.1038/10.1038/physci243037a0.

Rimmer, S.M., 2004. Geochemical paleoredox indicators in Devonian–Mississippian black shales, central Appalachian Basin (USA). Chem. Geol. 206, 373–391. https://doi.org/10.1016/j.chemgeo.2003.12.029.

Shanmugam, G., 1985. Significance of coniferous rain forests and related organic matter in generating commercial quantities of oil, Gippsland Basin, Australia. AAPG Bull. 69, 1241–1254.

Sinninghe Damsté, Jaap S., Frewin, N.L., Kenig, F., Leeuw, J.W.D., 1995. Molecular indicators for palaeoenvironmental change in a messinian evaporitic sequence (vena del gesso, italy). i: variations in extractable organic matter of ten cyclically deposited marl beds. Org. Geochem. 23 (6), 471–483. https://doi.org/10.1016/0146-6380(95)00040-L.

Stach, E., Mackowsky, M.T.H., Teichmüller, M., et al., 1982. Stach's Text Book of Coal Petrology, third ed. Gebruder Bomtraeger, Berlin, pp. 87–140. DOI:1224.

Stal, L.J., van Gemerden, H., Krumbein, W.E., 1985. Structure and development of a benthic marine microbial mat. FEMS (Fed. Eur. Microbiol. Soc.) Microbiol. Ecol. 31, 111–125. https://doi.org/10.1016/0378-1097(85)90007-2.

Summons, R.E., Jahnke, L.L., Hope, J.M., Logan, G.A., 1999. 2-methylhopanoids as biomarkers for cyanobacterial oxygenic photosynthesis. Nature 400 (6744), 554–557.

Sun, Xiuxiu, Cong, Haibing, Gao, Zhengjuan, et al., 2014. Movement Characteristics of Cyanobacteria Under Stress of Water-Lifting Aeration. Environ. Sci. https://doi.org/10.13227/j.hjkx.2014.05.020.

Volkman, J.K., 1986. A review of sterol markers for marine and terrigenous organic matter. Org. Geochem. 9 (2), 83–99. https://doi.org/10.1016/0146-6380(86)90089-6.

Volkman, J.K., 2003. Sterols in microorganisms. Appl. Microbiol. Biotechnol. 60, 495–506. https://doi.org/10.1007/s00253-002-1172-8.

Volkman, J.K., 2005. Sterols and other triterpenoids: source specificity and evolution of biosynthetic pathways. Org. Geochem. https://doi.org/10.1016/j.orggeochem.2004.06.013.

Volkman, J.K., Barrett, S.M., Dunstan, G.A., 1994. Sterol biomarkers for microalgae from the green algal class Prasinophyceae. Org. Geochem. 21, 1211–1218. https://doi.org/10.1016/0146-6380(94)90164-3.

Volkman, J.K., Barrett, S.M., Blackburn, S.I., 1998. Microalgal biomarkers: a review of recent research developments. Org. Geochem. 29, 1163–1179. https://doi.org/10.1016/s0146-6380(98)00062-x.

Walker, C.T., Price, N.B., 1963. Departure curves for computing paleosalinity from boron in illites and shales. Am. Assoc. Petrol. Geol. Bull. 47, 833–841. https://doi.org/10.1306/BC743A93-16BE-11D7-8645000102C1865D.

Wang, Tieguan, Zhong, Ningning, Hou, Dujie, et al., 1995. The role of bacteria in hydrocarbon generation mechanism in Banqiao depression. Sci. Sin. 100-107+116. DOI: CNKI:SUN:JBXK.0.1995-08-014.

Waples, D.W., 1985. Geochemistry in Petroleum Exploration. Human Resources and Develop. Co., Boston, inter, p. 232.

Xie, X., Borjigin, T., Zhang, Q., Zhang, Z., Qin, J., Bian, L., Volkman, J.K., 2015. Intact microbial fossils in the Permian Lucaogou Formation oil shale, Junggar Basin, NW China. Int. J. Coal Geol. 146, 166–178. https://doi.org/10.1016/j.coal.2015.05.011.

Zhang, Y., Sun, Y., Chen, J., 2020. Stable carbon isotope evidence for the origin of C_{28} steranes in lacustrine source rocks from the Qikou Sag, Bohai Bay Basin, Eastern China. Org. Geochem. 145, 104028. https://doi.org/10.1016/j.orggeochem.2020.104028.